Luminescence and energy-transfer mechanisms in Eu^{3+}-doped GaN epitaxial films

Shinya Higuchi,[1] Atsushi Ishizumi,[2] Junji Sawahata,[3] Katsuhiro Akimoto,[3] and Yoshihiko Kanemitsu[1,4,*]
[1]*Institute for Chemical Research, Kyoto University, Uji, Kyoto 611-0011, Japan*
[2]*Graduate School of Materials Science, Nara Institute of Science and Technology, Ikoma, Nara 630-0192, Japan*
[3]*Institute of Applied Physics, University of Tsukuba, Tsukuba, Ibaraki 305-8573, Japan*
[4]*Photonics and Electronics Science and Engineering Center, Kyoto University, Kyoto 615-8510, Japan*
(Received 31 July 2009; revised manuscript received 8 December 2009; published 21 January 2010)

We studied the photoluminescence (PL) and energy-transfer processes in Eu^{3+}-doped GaN epitaxial films by means of microscopic PL imaging spectroscopy. Eu^{3+}-doped GaN epitaxial films exhibited blue luminescence due to bound-exciton recombinations in GaN host crystals and red luminescence due to intra-4*f* transitions of Eu^{3+} ions. We found an anticorrelation between the exciton and Eu^{3+} PL intensities in space-resolved PL images, indicating that energy transfer from GaN crystals to Eu^{3+} ions determines the Eu^{3+} luminescence intensity. PL and PL excitation spectra showed that efficient Eu^{3+} luminescence is caused by two different excitation processes: energy transfer from the low-energy charge-transfer (CT) states to Eu^{3+} ions or from the delocalized states above the band edge of GaN crystals to Eu^{3+} ions. The energy-transfer process from the CT state to Eu^{3+} ions dominates the Eu^{3+} luminescence.

DOI: 10.1103/PhysRevB.81.035207 PACS number(s): 78.55.Cr, 61.72.uj, 81.05.Ea

I. INTRODUCTION

The doping of semiconductors with functional impurities is essential in semiconductor science and technology. Doped semiconductor bulk crystals and nanostructures show unique multifunctional properties beyond those of undoped bulk crystals and nanostructures.[1–4] Recently, much attention has been paid to wide band-gap semiconductors as new host crystals for doping of optical and magnetic active impurities, because they are expected to be highly efficient luminescence materials and room-temperature ferromagnetic materials.[5–24] In particular, nitrides and oxides such as GaN and ZnO crystals are excellent host materials for doping of transition-metal and rare-earth ions, and they have some advantages for light-emitting device applications.[5–16] These wide-gap host materials usually cause a significant reduction of the thermal quenching of the impurity luminescence, and they are transparent in a wide spectral range from red to blue. Rare-earth-doped GaN crystals have potential for application in full color monolithic devices. It has been reported that Tm-, Er-, and Eu-doped GaN films show blue, green, red, and infrared luminescence.[25–37] Stimulated light emission has also been reported in Eu^{3+}-doped GaN (GaN:Eu^{3+}) in the red spectral region.[38–40]

GaN:Eu^{3+} crystals exhibit efficient red luminescence due to intra-4*f* transitions of the Eu^{3+} ions under photoexcitation (photoluminescence, PL),[30,31] electron and hole injection (electroluminescence),[14,31–36] and electron-beam irradiation (cathodoluminescence).[37] Since the GaN host crystal is initially excited under those excitation conditions, energy transfer from the GaN host crystal to Eu^{3+} ions determines the red luminescence intensity of Eu^{3+} ions. GaN:Eu^{3+} crystals are a model material for studying energy-transfer mechanisms in wide-gap semiconductors doped with optically active impurities, and an understanding of the PL properties is very important from the point of view of both the fundamental physics and the development of high-performance optical devices. It has previously been reported that in GaN:Eu^{3+} epitaxial films there are two or more Eu^{3+} sites and the excitation process of Eu^{3+} ions is sensitive to Eu^{3+} sites.[41,42] In addition, space-resolved PL imaging spectroscopy has shown that the Eu^{3+} PL intensity depends on the monitored position in the GaN:Eu^{3+} epitaxial film with low Eu^{3+} concentration samples (1 at. % or less).[43,44] It has been demonstrated that microscopic PL imaging spectroscopy is one of the most versatile methods for investigating the detailed impurity-PL and energy-transfer mechanisms hidden by structural inhomogeneities.[43–45] However, the energy-transfer mechanism in GaN:Eu^{3+} films is not clear.

In this work, we study PL and energy-transfer processes in GaN:Eu^{3+} epitaxial films. GaN:Eu^{3+} films with 1 at. % Eu^{3+} concentration show the bound-exciton PL of GaN crystals in the blue spectral region and the Eu^{3+} PL in the red spectral region. From the PL excitation (PLE) spectra of blue and red PL bands, we conclude that Eu^{3+} ions doped in two different sites contribute to red PL. A fraction of doped Eu^{3+} ions form the low-energy charge-transfer (CT) state with GaN crystals, and Eu^{3+} ions are excited by energy transfer through the low-energy CT states. The remaining Eu^{3+} ions are excited by energy transfer from the delocalized band states above the band edge of GaN crystals to Eu^{3+} ions. Space-resolved PL imaging spectroscopy reveals that efficient red PL results from energy transfer through the CT state to Eu^{3+} ions.

II. EXPERIMENTAL

The samples used in this work were GaN:Eu^{3+} epitaxial films with an Eu^{3+} concentration of 1 at. %. The 1 at. % Eu^{3+} samples showed both strong and weak luminescent areas, and this inhomogeneity provides an opportunity for studying the energy-transfer mechanisms from the GaN crystal to Eu^{3+} ions using space-resolved PL imaging spectroscopy. The GaN:Eu^{3+} epitaxial films were grown on sapphire (0001) substrates by gas-source molecular-beam epitaxy using NH_3 gas as the nitrogen source.[46,47] The Eu^{3+} concentra-

 ©2010 The American Physical Society

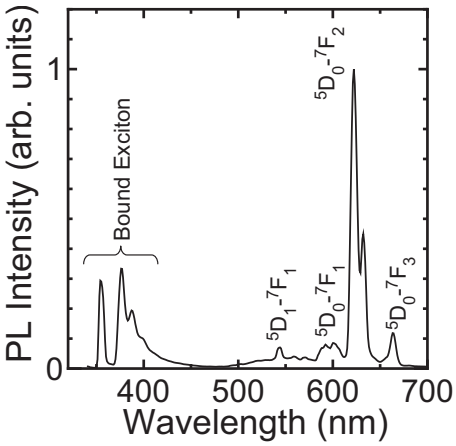

FIG. 1. PL spectrum of the GaN:Eu^{3+} epitaxial film with an Eu^{3+} concentration of 1 at. % under 325 nm light excitation at 14 K.

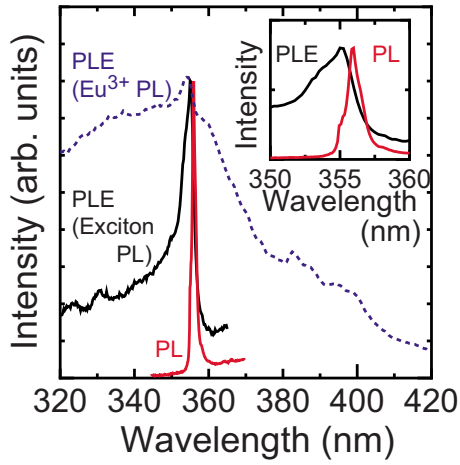

FIG. 2. (Color online) PLE spectra of the Eu^{3+} PL monitored at 622 nm (broken line) and of the bound-exciton PL monitored at 400 nm (solid line) at 20 K. The PL spectrum at the highest energy is shown under 325 nm excitation. The PL spectrum under 325 nm excitation and the PLE spectrum monitored at 400 nm are shown in the inset.

tions were determined from Rutherford backscattering spectrometry and energy dispersive x-ray spectroscopy.

For measurements of PL spectra, a He-Cd laser (325 nm; 3.81 eV) and a GaN laser diode (405 nm; 3.06 eV) were used as excitation sources. The PLE spectra were measured under monochromatic light excitation from a Xe lamp through a 25 cm monochromator. The PL signals were detected by a photomultiplier through a 25 cm monochromator. The spectral sensitivity of the measurement systems were calibrated using a standard tungsten lamp.

Space-resolved PL intensity images were obtained using a custom-built confocal optical microscope. A 325 nm He-Cd laser and a 405 nm GaN laser were used for excitation. The spatial resolution of this system using an objective lens with numerical aperture of 0.55 was approximately 1 μm. The PL signals from the samples were detected using a 50 cm monochromator and a cooled charge coupled device detector. The space-resolved PL decay profiles were measured using a 325 nm He-Cd laser modulated by an acoustic optical modulator. The signals were detected by a 25 cm monochromator equipped with a photomultiplier and were analyzed using an oscilloscope.

III. RESULTS AND DISCUSSION

A. GaN bound exciton and Eu^{3+} PL

Figure 1 shows the PL spectrum of the GaN:Eu^{3+} epitaxial film with 1 at. % Eu^{3+} concentration and excited with 325 nm light at 14 K. Many PL peaks are clearly observed in the visible spectral region. The most intense peak at 622 nm is assigned to the intra-4f transition ($^5D_0$-$^7F_2$) of Eu^{3+} ions.[42,43,46,47] PL peaks due to the $^5D_1$-$^7F_1$, $^5D_0$-$^7F_1$, and $^5D_0$-$^7F_3$ transitions of Eu^{3+} ions are also observed at around 544, 600, and 663 nm, respectively.[42]

The inset of Fig. 2 shows the highest-energy PL and PLE spectra of the GaN:Eu^{3+} film at 20 K. The energy of the PL peak is approximately 10 meV lower than the energy of free exciton of the GaN host crystal (the PLE peak energy). This Stokes shift shows that the PL peaks near the band edge of the GaN crystal are due to bound excitons, and not free excitons of the GaN host crystal. The highest-energy PL at 356 nm is associated with bound exciton at C impurities at Ga sites.[48] All PL peaks in the spectral range from ~370 nm to ~450 nm are due to bound excitons at C impurities on N sites and their phonon replicas.[48]

Figure 2 shows the PLE spectra of the bound-exciton PL at 400 nm and Eu^{3+} PL at 622 nm at 20 K. In the PLE spectrum for bound excitons, a sharp peak is clearly visible at 355 nm (3.49 eV), the energy of free excitons in the GaN host crystal. In the PLE spectrum of the Eu^{3+} PL, on the other hand, the PLE spectrum is much broader. The broad band appears at the low-energy region below the band gap of GaN crystals (i.e., around 390 nm). The doping of Eu^{3+} ions into GaN crystals produces low-energy states, below the band edge of the GaN crystal. Eu^{3+} ions are efficiently excited by energy transfer from the low-energy state of the GaN:Eu^{3+} crystal. The origin of the low-energy localized state below the GaN band-gap energy will be discussed below.

The Eu^{3+} PL spectral shape depends on the excitation wavelength. Figure 3 shows the PL spectra around 622 nm under excitation with (a) 325 and (b) 405 nm light at room temperature. The PL spectra in Fig. 3 are the space-averaged ones measured using conventional optics without an optical microscope. The above-band-gap excitation of the GaN crystal (i.e., where the photon energy is larger than the band-gap energy of the crystal) occurs under 325 nm light irradiation, while the low-energy state is directly excited by 405 nm light irradiation (the below-band-gap excitation). The Eu^{3+} PL spectrum at around 622 nm consists of several PL lines and the intensity ratio of these PL lines depends strongly on the excitation wavelength. Under the above-band-gap excitation (325 nm), the PL peaks denoted by indices α, β, and γ are observed. Under the below-band-gap excitation (405 nm), the peak β with a shoulder on the low-energy side is dominant, while the peaks α and γ are very weak. It is well

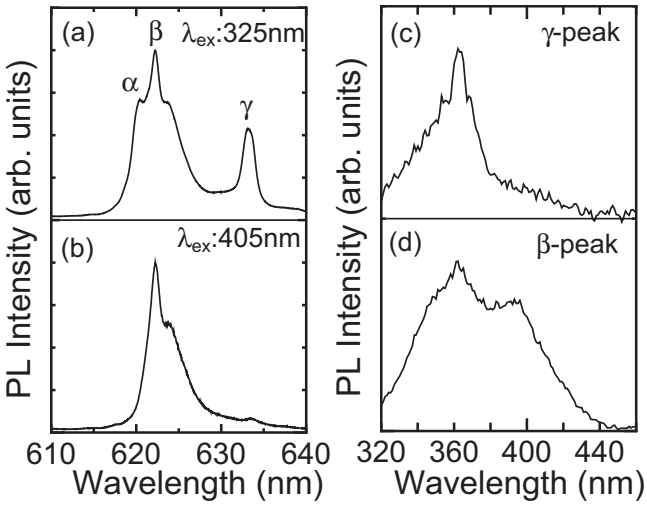

FIG. 3. PL spectra under (a) 325 nm and (b) 405 nm light excitation at room temperature. PLE spectra monitored at PL peak (c) γ and (d) β at room temperature.

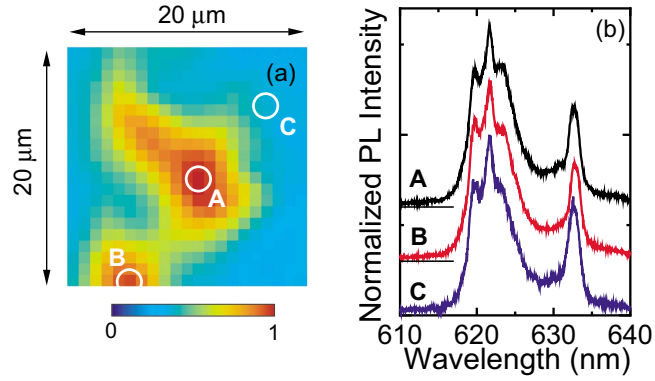

FIG. 4. (Color online) (a) Spatial image of the spectrally integrated Eu^{3+} PL intensity from 615 to 640 nm under 325 nm light excitation at room temperature. (b) Spatially resolved PL spectra monitored at positions A– C under 325 nm light excitation at room temperature.

known that the PL peaks due to the $^5D_0$-$^7F_2$ transition of Eu^{3+} ions are split and shifted by the crystal field around Eu^{3+} ions.[49,50] Therefore, the PL peaks, α, β, and γ, are attributed to the $^5D_0$-$^7F_2$ transition splitting and shifted by the crystal field. There are two or more Eu^{3+} sites in the local crystal field with different symmetry.

The PLE spectra monitored at the PL peak γ and β are shown in Figs. 3(c) and 3(d), respectively. The PLE spectrum at 300 K in Fig. 3(d) is different from that at 20 K in Fig. 2. The PL spectrum also depended on the measurement temperature. With a decrease of temperature, the PL peak α grew rapidly than the peak β and additional peaks appeared at around 620 nm. At low temperatures, nonradiative recombination rate of excitons in host GaN crystals is reduced, and exciton-related PL and defect PL bands appear. Since the exciton lifetime in the GaN host crystal becomes longer at low temperatures, direct energy transfer from the delocalized state in the GaN host crystal to Eu ions efficiently occurs. Then, it is believed that the PLE band near and above the band-edge energy of the GaN host crystal is enhanced at low temperatures as shown in Fig. 2. At room temperature, on the other hand, the intensity of the PL β peak is stronger than other PL peaks. The room-temperature PLE spectrum is useful for discussions on origin of Eu^{3+} PL peaks. In Fig. 3(c), the PLE spectrum of the PL peak γ shows clearly that the peak appears due to the above-band-gap excitation; Eu^{3+} ions having the PL peak γ are not excited by the below-band-gap excitation. Figure 3(d) shows that the PLE spectrum of the peak β consists of two broad bands; Eu^{3+} ions showing the PL peak β are excited by the below-band-gap excitation as well as the above-band-gap excitation. The PL peak β is caused by energy transfer from the low-energy states to Eu^{3+} ions. On the other hand, the PL peaks α and γ, are excited only by the above-band-gap excitation. Therefore, we conclude that there are two different excitation processes of Eu^{3+} ions.

The site-dependent PL spectrum and the broad low-energy band for the PLE spectrum strongly suggest the formation of the CT state below the band edge of GaN crystals. In many phosphor materials doped with rare-earth ions, such as Y_2O_3:Eu^{3+} and Y_2O_2S:Eu^{3+}, the broad PLE bands below the band-gap energy of the host material are attributed to the CT state, that is, electron transfer from an anion in the host crystal to a $4f$ orbital state of the rare-earth ion.[50–52] The energy of the CT state due to the Eu^{3+} ions, E^{CT}, is given by the equation, $E^{CT}=3.72(\eta-2)$, where η is the Pauling electronegativity of the anion.[53,54] When Eu^{3+} ions are doped into nitrides, E^{CT} is estimated to be about 3.5 eV.[54] Therefore, the broad PLE band around 390 nm (3.2 eV) can be explained by the formation of the CT state. It has been pointed out that defect states also contribute to the PLE band below the band-gap energy of the GaN host crystals.[30,41,42,55] Because defect states usually act as nonradiative recombination centers, we believe that the PLE band results mainly from the CT state rather than the defects, which is similar to the case of Eu^{3+}-doped oxides. We conclude that the CT state is due to Eu^{3+} ions incorporated into substitutional Ga sites, while other Eu^{3+} ions are located in interstitial sites and electronically isolated from GaN with no strong interactions.

B. Spatially resolved PL imaging spectroscopy

In the above discussion, we have shown that, in GaN:Eu^{3+} epitaxial films, there are two Eu^{3+} sites contributing to red luminescence, and the excitation efficiency of the Eu^{3+} ions is sensitive to the energy-transfer process. Microscopic PL imaging spectroscopy is used to clarify the origin of the site-dependent Eu^{3+} PL. Figure 4(a) shows a two-dimensional image of spectrally integrated PL intensity from 615 to 640 nm under 325 nm light excitation at room temperature. Figure 4(b) shows the spatially resolved PL spectra monitored at positions A–C in Fig. 4(a). The PL peaks α, β, and γ are observed at all the monitored positions, similar to the PL spectrum in Fig. 3(a). This is because even in microscopic spectroscopy there exist different Eu^{3+} sites in the spot of the excitation laser whose diameter is ~ 1 μm. We found that the peak energies of three peaks do not depend on the monitored position. However, the intensity of the peak β

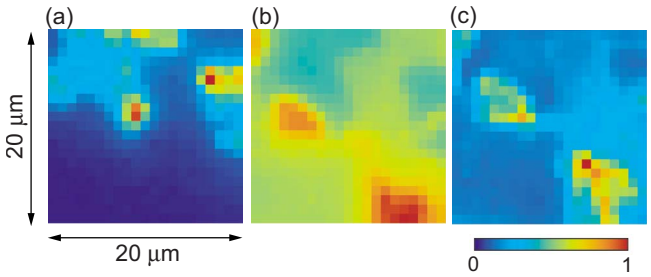

FIG. 5. (Color online) (a) Spatial image of the intensity of the bound-exciton PL monitored in the spectral range from 350 to 360 nm under 325 nm light excitation at 10 K. Spatial images of the PL intensity due to $^5D_0$-$^7F_2$ transition of Eu^{3+} ions monitored in the spectral range from 615 to 640 nm under (b) 325 and (c) 405 nm light excitation at 10 K.

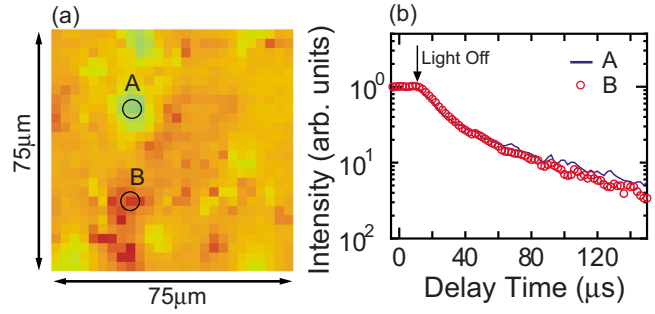

FIG. 6. (Color online) (a) Spatial image of the PL intensity due to $^5D_0$-$^7F_2$ transition of the GaN:Eu^{3+} epitaxial film under 325 nm light excitation at 10 K. (b) Spatially resolved PL decay profiles monitored at positions A (solid line) and B (open circles) under 325 nm light excitation at 10 K.

is high at the bright positions.[43] The Eu^{3+} ions forming the CT state show efficient luminescence.

At low temperatures, both GaN exciton-related PL and Eu^{3+}-related PL bands are clearly observed. To clarify the energy transfer from the GaN host crystal to Eu^{3+} ions, we measured two-dimensional images of exciton- and Eu^{3+}-related PL intensities. The intensity ratio of these two PL is useful for discussions on energy-transfer processes. Here, we show spectrally integrated PL data at low temperatures, because many peaks are spectrally overlapped at around the β peak at low temperatures. Figure 5(a) shows a two-dimensional image of the PL intensity due to bound excitons of the GaN host crystal, where the PL is monitored in the spectral range from 350 to 360 nm under 325 nm light excitation at 10 K. Figures 5(b) and 5(c) show two-dimensional images of the PL intensity at 10 K due to the Eu^{3+} ions under (b) 325 nm and (c) 405 nm light excitation, where the Eu^{3+} PL is monitored in the spectral range from 615 to 640 nm. All PL images were obtained in the same area. We find a good anticorrelation between the bound exciton and Eu^{3+} PL in the spatial images. The intensity of the PL due to bound excitons is strong at the positions where the Eu^{3+} PL is very weak. This indicates that the reduction of the bound-exciton PL is caused by energy transfer from the GaN host crystal to Eu^{3+} ions.

From a comparison of the spatial images between Eu^{3+} PL intensities under 325 nm and 405 nm excitation, we find that the difference between bright and dark positions is enhanced by the 405 nm light, but there is a good correlation between these two images. If the bright and dark positions in the PL images are attributed to the high and low Eu^{3+} concentration areas, respectively, the difference between bright and dark positions would be independent of the excitation wavelength. Therefore, our observations show that the spatial inhomogeneity of the PL images is not caused by the spatial fluctuation of the Eu^{3+} concentration. Because the 405 nm laser only excites the CT state below the band gap of the GaN crystal, the PL image under 405 nm excitation (the below-band-gap excitation) displays the spatial distribution of Eu^{3+} ions forming the CT state. On the other hand, under 325 nm excitation (the above-band-gap excitation), the GaN host crystal is initially excited by laser light, and then energy transfer from the host crystal to Eu^{3+} ions occurs. Both the isolated Eu^{3+} and CT state Eu^{3+} ions can be excited by the energy transfer under 325 nm excitation, resulting in a low contrast PL image. Eu^{3+} ions are uniformly dispersed in the entire sample, while Eu^{3+} ions forming CT states are spatially localized. If the efficiency of Eu^{3+} PL via the CT state is poor, there would be no correlation between PL images under 325 and 405 nm excitation. From good correlation between two images, we can point out that Eu^{3+} ions in CT states show efficient luminescence even under the above-band-gap excitation of the GaN host crystal.

Red luminescence is caused by the intra-4f transitions of Eu^{3+} ions, and the Eu^{3+} PL intensity is sensitive to the local crystal field. The electric-dipole intra-4f transitions become partially allowed due to mixing with orbitals having different parity[50] because the local crystal field around the Eu^{3+} ions is distorted by the point defect. In this case, enhancement of the radiative decay rate of Eu^{3+} ions should occur around the point defects and cause the intense Eu^{3+} PL. Inhomogeneous spatial distribution of nonradiative centers is also able to cause the spatial fluctuation of the Eu^{3+} PL intensity. In order to study the radiative and nonradiative decay rate of the Eu^{3+} ions with different local environments, we measured PL decay profiles at different positions in space-resolved PL images.

Figure 6(a) shows the spatial image of the Eu^{3+} PL intensity under 325 nm cw laser excitation. Figure 6(b) shows the space-resolved PL decay profiles under 325 nm chopped excitation at positions A and B indicated in Fig. 6(a). For measurements of the PL decay profiles, we used a rectangular light pulse. A plateau in Fig. 6(b) is the PL intensity during light irradiation. After the light is off, the PL intensity decays. A multiexponential decay of the intensity is observed. The Eu^{3+} PL intensity at the position A is weak, while that at the position B is strong. However, there is no significant difference between the PL decay profiles monitored at positions A and B. In fact, we cannot clearly observe the spatial distribution of the PL decay time under our experimental resolutions. This implies that the intense Eu^{3+} PL at the bright position cannot be explained by the enhancement of the radiative decay rate and/or by the reduction of the nonradiative decay rate.

To investigate local distortion of the host crystal, we measured the spatial images of Eu^{3+} PL intensity due to magnetic

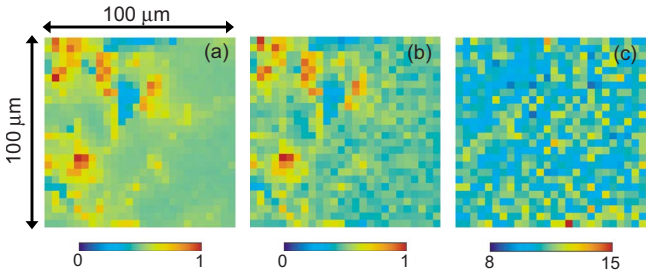

FIG. 7. (Color online) Spatial images of the PL intensity due to (a) $^5D_0$-$^7F_2$ and (b) $^5D_0$-$^7F_1$ transitions of Eu^{3+} ions under 325 nm light excitation at 10 K. (c) Spatial image of the PL intensity ratio of the $^5D_0$-$^7F_2$ to $^5D_0$-$^7F_1$ transition.

dipole allowed $^5D_0$-$^7F_1$ transitions and electric dipole allowed $^5D_0$-$^7F_2$ transitions. Because the PL intensity due to the magnetic-dipole transition is insensitive to the site symmetry,[50] the spatial variation of the distortion of the host crystals is displayed by the PL intensity ratio of the electric-dipole transition to the magnetic-dipole transition. Figure 7 shows the spatial images of the PL intensity due to (a) the $^5D_0$-$^7F_2$ and (b) $^5D_0$-$^7F_1$ transitions under 325 nm light excitation at 10 K. The PL intensities due to the $^5D_0$-$^7F_2$ and $^5D_0$-$^7F_1$ transitions are monitored in the spectral range from 615 nm to 640 nm, and in the spectral range from 585 to 615 nm, respectively. Figure 7(c) shows the spatial image of the intensity ratio of the $^5D_0$-$^7F_2$ transition to the $^5D_0$-$^7F_1$ transition. The PL intensity images of the magnetic and electric-dipole transitions are almost the same. Therefore, we conclude that the distortion of the host crystals is uniform within the spatial resolution of our system, and that the strong Eu^{3+} PL is not caused by the enhancement of the $^5D_0$-$^7F_2$ transition rate due to the crystal-field distortion. Furthermore, the Eu^{3+} PL peak energies are independent of the monitored position. This result also shows the spatial uniformity of the distortion of the host crystals.

Spatially resolved PL imaging spectroscopy confirmed that the intensity of the Eu^{3+} PL is not sensitive to the radiative and nonradiative processes of excited Eu^{3+} ions. As mentioned above, there exist different Eu^{3+} sites in the spot of the excitation laser and the spatially resolved spectroscopic data do not reflect PL properties of a single Eu^{3+} site. Figures 6 and 7 show that the efficiency of the Eu^{3+} PL is dominated by the energy transfer from GaN crystals to Eu^{3+} ions. Since the efficient energy transfer via the low-energy localized state causes the efficient red PL due to intra-4f transitions of Eu^{3+} ions, the formation of the CT state due to the interaction between Eu^{3+} ions and GaN crystals is essential for the efficient Eu^{3+} PL. The formation of the CT state is clearly observed as the broad band in the PLE spectrum, as shown in Figs. 2 and 3(d). After photoexcitation of carriers in the GaN host, carriers are relaxed into the low-energy CT state, and then Eu^{3+} ions are excited via the low-energy CT state.

From spectroscopic data, we conclude that there are two different sites for light-emitting Eu^{3+} ions: the CT state (peak β) and isolated Eu^{3+} ions (peak α and γ). In the PLE spectrum, the PL peaks α and γ are observed only under the above-band-gap excitation, but peak β is observed even under the below-band-gap excitation. These data shows that excitons are delocalized near isolated Eu^{3+} ions, but localized in the CT states. There are two excitation mechanisms. One is the excitation of Eu^{3+} ions through the CT state. The other is the direct energy transfer from delocalized excitons to isolated Eu^{3+} ions. Both the delocalized exciton after photoexcitation and the localized exciton at the CT states play an essential role in excitation processes of Eu^{3+} ions.

IV. CONCLUSION

In this work, we studied PL and energy-transfer mechanisms of GaN:Eu^{3+} (1 at. % Eu^{3+}) epitaxial films. The GaN:Eu^{3+} epitaxial films exhibit red luminescence due to the Eu^{3+} ions and blue luminescence due to bound excitons at low temperatures. The PL intensity due to the Eu^{3+} and bound excitons is sensitive to the monitored position in the microscopic PL imaging spectroscopy. Two excitation processes of Eu^{3+} ions contribute to red luminescence: a fraction part of the Eu^{3+} ions produce the CT states, through electron transfer from an anion in the GaN host crystals into a 4f orbital state of Eu^{3+} ions. The remaining Eu^{3+} ions are isolated, because there is no strong electronic interaction between Eu^{3+} ions and GaN crystals. Efficient energy transfer occurs thorough the CT states at room temperature. Moreover, we found no enhancement of the radiative decay rate and no change in the magnetic and electric-dipole transitions between the bright and dark position in the PL images. This finding shows that the Eu^{3+} PL intensity is not sensitive to the radiative and nonradiative recombination processes of excited Eu^{3+} ions and the energy transfer from the GaN host crystals to the Eu^{3+} ions determines the Eu^{3+} PL intensity.

ACKNOWLEDGMENTS

Part of this work was supported by JSPS KAKENHI (Grant No. 21340084) and MEXT KAKENHI (Grant No. 20104006), and the Kyoto University G-COE program from MEXT of Japan.

*Corresponding author. kanemitu@scl.kyoto-u.ac.jp

[1] D. J. Norris, Al. L. Efros, and S. C. Erwin, Science **319**, 1776 (2008).
[2] R. Beaulac, P. I. Archer, S. T. Ochsenbein, and D. R. Gamelin, Adv. Funct. Mater. **18**, 3873 (2008).
[3] A. J. Steckl, J. H. Park, and J. M. Zavada, Mater. Today **10**, 20 (2007).
[4] T. Dietl, H. Ohno, F. Matsukura, J. Cibert, and D. Ferrand, Science **287**, 1019 (2000).
[5] S. Kim, S. J. Rhee, X. Li, J. J. Coleman, and S. G. Bishop, Phys.

Rev. B **57**, 14588 (1998).
[6] O. Contreras, S. Srinivasan, F. A. Ponce, G. A. Hirata, F. Ramos, and J. McKittrick, Appl. Phys. Lett. **81**, 1993 (2002).
[7] Y. Nakanishi, A. Wakahara, H. Okada, A. Yoshida, T. Ohshima, and H. Itoh, Appl. Phys. Lett. **81**, 1943 (2002).
[8] J. H. Kim and P. H. Holloway, J. Appl. Phys. **95**, 4787 (2004).
[9] S. Shirakata, R. Sasaki, and T. Kataoka, Appl. Phys. Lett. **85**, 2247 (2004).
[10] Q. L. Liu, Y. Bando, F. F. Xu, and C. C. Tang, Appl. Phys. Lett. **85**, 4890 (2004).
[11] A. Ishizumi and Y. Kanemitsu, Appl. Phys. Lett. **86**, 253106 (2005).
[12] T. Andreev, Y. Hori, X. Biquard, E. Monroy, D. Jalabert, A. Farchi, M. Tanaka, O. Oda, Le Si Dang, and B. Daudin, Phys. Rev. B **71**, 115310 (2005).
[13] J. Sawahata, J. Seo, S. Chen, M. Takiguchi, D. Saito, S. Nemoto, and K. Akimoto, Appl. Phys. Lett. **89**, 192104 (2006) and references therein.
[14] A. Nishikawa, T. Kawasaki, N. Furukawa, Y. Terai, and Y. Fujiwara, Appl. Phys. Express **2**, 071004 (2009).
[15] Y. D. Glinka, H. O. Everitt, D. S. Lee, and A. J. Steckl, Phys. Rev. B **79**, 113202 (2009), and references therein.
[16] L. Bodiou, A. Braud, J.-L. Doualan, R. Moncorgé, J. H. Park, C. Munasinghe, A. J. Steckl, K. Lorenz, E. Alves, and B. Daudin, J. Appl. Phys. **105**, 043104 (2009).
[17] H. J. Lozykowski, W. M. Jadwisienczak, J. Han, and I. G. Brown, Appl. Phys. Lett. **77**, 767 (2000).
[18] M. L. Reed, N. A. El-Masry, H. H. Stadelmaier, M. K. Ritums, M. J. Reed, C. A. Parker, J. C. Roberts, and S. M. Bedair, Appl. Phys. Lett. **79**, 3473 (2001).
[19] M. Hashimoto, A. Yanase, R. Asano, H. Tanaka, H. Bang, K. Akimoto, and H. Asahi, Jpn. J. Appl. Phys. **42**, L1112 (2003).
[20] J. B. Gruber, U. Vetter, H. Hofsäss, B. Zandi, and M. F. Reid, Phys. Rev. B **70**, 245108 (2004).
[21] J. Hite, G. T. Thaler, R. Khanna, C. R. Abernathy, S. J. Pearton, J. H. Park, A. J. Steckl, and J. M. Zavada, Appl. Phys. Lett. **89**, 132119 (2006).
[22] K. R. Kittilstved, W. K. Liu, and D. R. Gamelin, Nature Mater. **5**, 291 (2006).
[23] A. Ney, T. Kammermeier, V. Ney, S. Ye, K. Ollefs, E. Manuel, S. Dhar, K. H. Ploog, E. Arenholz, F. Wilhelm, and A. Rogalev, Phys. Rev. B **77**, 233308 (2008).
[24] S. Taguchi, A. Ishizumi, T. Tayagaki, and Y. Kanemitsu, Appl. Phys. Lett. **94**, 173101 (2009).
[25] J. D. MacKenzie, C. R. Abernathy, S. J. Pearton, U. Hömmerich, J. T. Seo, R. G. Wilson, and J. M. Zavada, Appl. Phys. Lett. **72**, 2710 (1998).
[26] R. Birkhahn and A. J. Steckl, Appl. Phys. Lett. **73**, 2143 (1998).
[27] K. Hara, N. Ohtake, and K. Ishii, Phys. Status Solidi B **216**, 625 (1999).
[28] H. J. Lozykowski, W. M. Jadwisienczak, and I. Brown, Appl. Phys. Lett. **74**, 1129 (1999).
[29] A. J. Steckl, M. Garter, D. S. Lee, J. Heikenfeld, and R. Birkhahn, Appl. Phys. Lett. **75**, 2184 (1999).
[30] Z. Li, H. Bang, G. Piao, J. Sawahata, and K. Akimoto, J. Cryst. Growth **240**, 382 (2002).
[31] S. Morishima, T. Maruyama, M. Tanaka, Y. Masumoto, and K. Akimoto, Phys. Status Solidi A **176**, 113 (1999).
[32] A. J. Steckl, J. Heikenfeld, D. S. Lee, and M. Garter, Mater. Sci. Eng., B **81**, 97 (2001).
[33] D. S. Lee, J. Heikenfeld, R. Birkhahn, M. Garter, B. K. Lee, and A. J. Steckl, Appl. Phys. Lett. **76**, 1525 (2000).
[34] J. Heikenfeld, M. Garter, D. S. Lee, R. Birkhahn, and A. J. Steckl, Appl. Phys. Lett. **75**, 1189 (1999).
[35] D. S. Lee and A. J. Steckl, Appl. Phys. Lett. **80**, 1888 (2002).
[36] Y. Q. Wang and A. J. Steckl, Appl. Phys. Lett. **82**, 502 (2003).
[37] M. Tanaka, S. Morishima, H. Bang, J. S. Ahn, T. Sekiguchi, and K. Akimoto, Phys. Status Solidi C **0**, 2639 (2003).
[38] J. H. Park and A. J. Steckl, Appl. Phys. Lett. **85**, 4588 (2004).
[39] J. H. Park and A. J. Steckl, J. Appl. Phys. **98**, 056108 (2005).
[40] J. H. Park and A. J. Steckl, Appl. Phys. Lett. **88**, 011111 (2006).
[41] E. E. Nyein, U. Hömmerich, J. Heikenfeld, D. S. Lee, A. J. Steckl, and J. M. Zavada, Appl. Phys. Lett. **82**, 1655 (2003).
[42] H. Peng, C.-W. Lee, H. O. Everitt, C. Munasinghe, D. S. Lee, and A. J. Steckl, J. Appl. Phys. **102**, 073520 (2007); H. Y. Peng, C. W. Lee, H. O. Everitt, D. S. Lee, A. J. Steckl, and J. M. Zavada, Appl. Phys. Lett. **86**, 051110 (2005).
[43] A. Ishizumi, J. Sawahata, K. Akimoto, and Y. Kanemitsu, Appl. Phys. Lett. **89**, 191908 (2006).
[44] A. Ishizumi, J. Sawahata, K. Akimoto, and Y. Kanemitsu, Mater. Sci. Eng., B **146**, 186 (2008).
[45] A. Ishizumi and Y. Kanemitsu, J. Phys. Soc. Jpn. **78**, 083705 (2009).
[46] J. Sawahata, J. W. Seo, S. Chen, and K. Akimoto, Phys. Status Solidi A **205**, 71 (2008).
[47] H. Bang, S. Morishima, J. Sawahata, J. Seo, M. Takiguchi, M. Tsunemi, K. Akimoto, and M. Nomura, Appl. Phys. Lett. **85**, 227 (2004).
[48] M. A. Reshchikov and H. Morkoç, J. Appl. Phys. **97**, 061301 (2005).
[49] A. A. Kaminskii, *Laser Crystals*, 2nd ed., Springer Series in Optical Science (Springer, Berlin, 1990), Vol. 14.
[50] *Phosphor Handbook*, edited by S. Shionoya and W. M. Yen (CRC Press, Boca Raton, FL, 1999).
[51] R. C. Ropp, J. Electrochem. Soc. **112**, 181 (1965).
[52] C. W. Struck and W. H. Fonger, J. Lumin. **1-2**, 456 (1970).
[53] P. Dorenbos, J. Lumin. **111**, 89 (2005).
[54] P. Dorenbos and E. van der Kolk, Appl. Phys. Lett. **89**, 061122 (2006).
[55] C.-W. Lee, H. O. Everitt, D. S. Lee, A. J. Steckl, and J. M. Zavada, J. Appl. Phys. **95**, 7717 (2004).